Quantising a generic family of billiards with analytic boundaries

1984 J. Phys. A: Math. Gen. 17 1049

(http://iopscience.iop.org/0305-4470/17/5/027)

J. Phys. A: Math. Gen. **17** (1984) 1049–1074. Printed in Great Britain

Quantising a generic family of billiards with analytic boundaries

Marko Robnik

Astronomische Institute, SFB 131—Radioastronomie, Universität Bonn, Auf dem Hügel 71, D-5300 Bonn, FRG

Received 10 August 1983

Abstract. A generic family of plane billiards has been discovered recently. The shape of the boundary is given by the quadratic conformal image of the unit circle, and is thus real analytic. For small deformations of the unit disc the billiard is a typical KAM system, but becomes ergodic or even mixing when the curvature of the boundary vanishes at some point. The Kolmogorov entropy has been calculated, and it increases with the deformation of the boundary.

In the present work we study aspects of the quantum chaos for this billiard. We solve numerically the eigenvalue problem for the Laplace operator with Dirichlet's boundary condition. We examine the spectrum, and inspect the avoided crossings at which mixing of nearby states occurs. The variation of the nodal structure and of the localisation properties of the eigenfunctions is studied. In analysing the level spacing distribution we find a continuous transition from the Poisson distribution towards the Wigner distribution. The exponent in the level repulsion law varies continuously along with a generic perturbation. For small perturbations it seems to be proportional to the square root of the perturbation parameter.

1. Introduction

The purpose of this work is to examine some general ideas on quantum chaos in a family of simple but generic Hamilton systems. More precisely, we study numerically the Dirichlet eigenvalue problem for the Laplace operator on a plane billiard with analytic boundaries. The shape of the billiard is defined by a quadratic conformal map of the unit disc. The classical dynamics of this system has been studied recently (Robnik 1983), and it has been shown that the family of billiards thus defined is indeed a generic class of Hamilton systems: in one extreme it is an integrable system (circular disc), becoming a KAM system for small perturbations, and finally, in another extreme, it is (most probably) a mixing or even a Bernoulli system (Strelcyn 1983, Robnik 1984). The system shows thus a generic stochastic transition, and if there exists any well defined analogy between the classical and quantum chaos, then it must be revealed in this case.

We shall solve the eigenvalue problem and observe how the energy levels and the corresponding eigenfunctions change as the family parameter is varying. Similar work on a classical chaotic system has been done by McDonald and Kaufman (1979). They studied the eigenvalue problem for the stadium. Berry (1981) has quantised Sinai's billiard. Very recently two groups have studied non-generic families of billiards that are (for all parameter values) infinitely close to a pseudointegrable system. Berry and

0305-4470/84/051049+26$02.25

Wilkinson (1983) investigated the triangles, while Lewis *et al* (1984) studied the parallelograms.

When an attempt is made to draw an analogy between the (very precisely defined) classical chaos and (not so well defined) quantum chaos, the following comments should be taken into account.

(C1) The classical chaos is a consequence of *nonlinearity* and *nonintegrability*, and its ultimate origin is the (exponential) divergence of nearby orbits.

(C2) There are two major and general aspects of the classical chaos. The first is the *dynamical* point of view, according to which chaos means unpredictability of the classical motion, which has (to the given degree) statistical properties as the only predictable attributes. The ergodic theory (Sinai 1976, Arnold and Avez 1968, Helleman 1980, Berry 1983a) gives a precise classification of the different levels from the hierarchy of chaotic motion (almost integrable, ergodic, mixing, Bernoulli, etc). (This is the reason for saying that the classical chaos has a very precise meaning.) The second aspect is the *structural* point of view, according to which chaos means a certain kind of (loss of) structure of the phase portrait. For instance, the integrable systems are characterised by the existing invariant tori, in KAM systems the tori are broken in resonant gaps, K systems are predominantly chaotic, but may have small stability islands, ergodic and mixing systems are structureless. This second point of view is able to distinguish clearly between integrable and nonintegrable cases, but cannot distinguish between the ergodic and mixing systems for example.

(C3) The dynamical picture of classical chaos corresponds to the evolution of quantum states (and the (un)expected quantum chaos). But there are some fundamental difficulties: firstly, quantum mechanics is a *linear* theory; secondly, the Hamilton operator of a bound system has always a *discrete* spectrum and the quantum motion is thus always *quasiperiodic*, as opposed to the possibility of a continuous spectrum of the Liouville operator in classical mechanics. Indeed, having a discrete countable basis in Hilbert space, one can represent the quantum motion as the motion of an infinite collection of *uncoupled* one-dimensional harmonic oscillators. It does not surprise us that each state is recurrent in time (Hogg and Huberman 1982).

There is no analogy of the exponential divergence of orbits, and hence no analogy of classical chaotic motion. Of course, by introducing external perturbations, or by coupling to a continuum, one might very well find a chaotic behaviour, but not a self-generated one.

(C4) However, the structural point of view of the classical chaos allows us to draw analogies, and to obtain an idea of what are the implications of nonintegrability in quantum mechanics. The most important structural change in the classical phase space when an integrable system is perturbed, and becomes e.g. ergodic, is the destruction of invariant tori. The projection of a classical torus is generally a proper subset of the energetically accessible region, so that the corresponding motion in configuration space is localised, i.e. bounded, on a smaller than possible region. But if a torus is broken, and if the motion becomes ergodic on the energy surface in phase space, then the trajectories in configuration space fill the entire region admitted by the condition that the energy is larger than the potential. One important consequence of the structural changes along with the transition to chaos is thus the delocalisation of the classical motion.

In quantum mechanics a certain analogy of phase space exists, and using the Wigner functions it has been possible to explain these structural changes more quantitatively, in particular by using the semiclassical approach (Berry 1983, and references therein).

Indeed, increasingly more emphasis seems to be given to this structural point of view when the stationary problem of nonintegrable quantum systems is studied (Hose and Taylor 1983). Two aspects seem most important. (i) If a quantum system is nonintegrable the wavefunctions in configuration space appear to be random. (ii) As a consequence of this the transition probabilities are expected to decrease drastically and to become randomly distributed. These postulates give very definite predictions as concerns, for instance, atomic and molecular spectra. The quadratic Zeeman effect is an example (Robnik 1981, 1982, Clark and Taylor 1980, Harada and Hasegawa 1983).

On the other hand, if a system happens to be integrable, then the wavefunctions in configuration space are expected to be localised, in close analogy to the localisation of the classical trajectories. Hose and Taylor (1983) call it surprising (or unexpected) localisation, because the measure of the Hamilton systems having this property is zero. Nevertheless, the localisation of states in the above sense can be generally expected for low levels. This might be an *a priori* qualitative explanation for the stability of molecules. Examples in this context can be found in the review by Noid *et al* (1981a, b).

These comments give only a rough, introductory idea of what are the most important structural changes implied by the nonintegrability, and which might be called quantum chaos. Our results support the following general ideas on quantum chaos.

(i) The repulsion of energy levels and the existence of avoided crossings is a property of nonintegrable systems (Ramaswamy and Marcus 1981, Berry 1983a, Zaslavsky 1981, Marcus 1980a, b).

(ii) As a consequence of (i) the distribution of level spacings is similar to the Wigner distribution (Zaslavsky 1977, 1979, 1981, Berry 1981).

(iii) Strong mixing of states occurs near the avoided crossings (Noid *et al* 1980, 1981a, b, Marcus 1980a, b, Ramaswamy and Marcus 1981).

(iv) As a consequence of (iii) the wavefunctions of levels participating in an avoided crossing have a random appearance (McDonald and Kaufman 1979, Noid *et al* 1979).

(v) If there are many avoided crossings, then the transition probabilities are notably diminished and randomly distributed (see also Marcus 1980a).

(vi) For sufficiently small perturbations of an integrable system some levels follow the predictions of the perturbation theory, while others do not. The former states correspond to the most stable classical tori through the EBK quantisation (Ramaswamy and Marcus 1981).

(vii) The lower levels and the associated wavefunctions show little or no features described in (i)–(v), and are thus always regular.

In the following we examine the spectrum of our billiard box (§ 4) and analyse the nodal structure and the localisation properties of the eigenfunctions (§ 5). In § 6 we investigate the level spacing distribution $P(S)$ and the associated law of level repulsion. Emphasis is put on the variation of these properties with the deformation of the billiard. In particular, we find a continuous transition of $P(S)$ from the Poisson distribution (integrable case) to the Wigner distribution (ergodic system).

2. The definition of the family of billiards

The shape of our billiard is shown in figure 1. It is defined as a quadratic conformal map (in the complex w-plane) of the unit disc (in the complex z-plane), i.e.

$$w = Az + Bz^2. \tag{1}$$

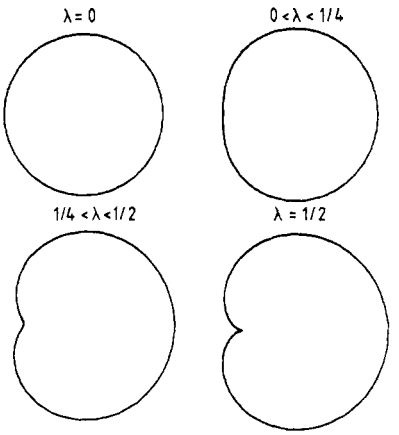

Figure 1. The shape of the billiard at various values of λ.

In real notation ($w =: u + iv$, $z =: x + iy$) we have the parametric equation of the boundary,

$$u = A\cos\theta + B\cos 2\theta, \qquad v = A\sin\theta + B\sin 2\theta, \tag{2}$$

where θ is the polar angle in the z plane. We shall denote $\lambda := B/A$. Then for $\lambda = 0$ we have a circular disc, for $\lambda = \frac{1}{4}$ the curvature vanishes at $\theta = \pi$, and for $\lambda = \frac{1}{2}$ the derivative dw/dz vanishes at the boundary (at $\theta = \pi$), so that $z \mapsto w(z)$ is no longer a conformal map and a cusp occurs there. The area of our billiard is equal to

$$\mathcal{A} = \pi(A^2 + 2B^2). \tag{3}$$

With the reparametrisation

$$A = \cos p, \qquad B = (1/\sqrt{2})\sin p, \tag{4}$$

$$p = \tan^{-1}(\lambda\sqrt{2}), \tag{5}$$

for $0 \leqslant p \leqslant p_{\text{sing}} = \tan^{-1}(1/\sqrt{2})$ we have a continuous family of billiards of constant area equal to $\mathcal{A} = \pi$.

The reasons for choosing this particular family of billiards are the following.

(a) Most of the rigorous theorems on the classical dynamics of billiards assume smooth boundaries (Lazutkin 1973, Mather 1982, Strelcyn 1982). Hence the need for analyticity.

(b) It is convenient to take a conformal map of the unit disc. Firstly, because this is sometimes useful in calculating the classical orbits; secondly, because we obtain at the same time an equivalent and interesting system in the unit disc with conformally transformed kinetic energy. For example, the trajectories on the unit disc, which are conformal maps of the orbits of our billiard, are hyperbolae. Thirdly, as can be seen from (2), the boundary of our billiard is determined by the lowest harmonic perturbation of the unit circle. This may be generalised by including higher harmonic perturbations. Finally, and this is most important, the conformal map enables us to solve the Dirichlet eigenvalue problem for the (conformally transformed) Laplace operator on the unit disc, where we have the basis of Bessel functions and can use the diagonalisation method.

(c) The choice of the quadratic map is motivated, of course, by simplicity arguments.

As far as the classical dynamics is concerned, it is not surprising that this family is indeed interesting (Robnik 1983, henceforth referred to as (I)). A theorem by Mather (1982) predicts the disappearance of Lazutkin's tori (1973) as soon as the curvature of the boundary vanishes at least at one point. In our case this happens at $\lambda = \frac{1}{4}$ and one should expect a chaotic behaviour for $\frac{1}{4} \leq \lambda < \frac{1}{2}$. Indeed, it has been shown in (I) that our billiard is a generic classical Hamilton system. It is integrable for $\lambda = 0$ (conservation of angular momentum), and becomes a typical KAM system for small λ. It has several stable periodic orbits surrounded by quite large stability islands, as can be seen in the Poincaré maps published in (I). The most important stable periodic orbit is the horizontal period-two orbit, corresponding to the simple bouncing between the points $\theta = 0$ and $\theta = \pi$. It has the stability interval $\lambda \in [0, \frac{1}{2}(\sqrt{2}-1)]$. At $\lambda = (\sqrt{2}-1)/2$ it goes unstable, and bifurcates. A cascade of period doubling bifurcations follows, with the accumulation point $\lambda \leq \frac{1}{4}$. At $\lambda > \frac{1}{4}$ no tori or stability islands are seen in the Poincaré maps. Moreover, the investigation of the homoclinic points indicates that the system has mixing properties. Also, the Kolmogorov entropy increases very rapidly as λ increases through $\lambda = \frac{1}{4}$. It might be conjectured that the system is not only mixing, but even Bernoulli for $\lambda \in [\frac{1}{4}, \frac{1}{2})$ (Strelcyn 1983, Robnik 1984). There is strong numerical evidence for the mixing property.

3. Quantising the billiard: Dirichlet's eigenvalue problem for the Laplace operator

In this section we shall formulate the eigenvalue problem. Let $D(p)$ denote the domain of our billiard whose boundary in the real (u, v)-plane is given by (2) and (4). Then, studying the quantum states of a point particle inside this two-dimensional box, we have the Hamilton operator $\hat{H} = -\Delta_{uv} = -(\partial^2/\partial u^2 + \partial^2/\partial v^2)$, where Δ_{uv} is the Laplace operator, and we assume $\hbar^2/2m = 1$. The Hilbert space on which $\hat{H} = -\Delta_{uv}$ is operating is the set of all functions ψ defined on $D(p)$ and obeying the Dirichlet boundary condition, i.e. $\psi = 0$ on $\partial D(p)$. The eigenvalue problem that we are going to solve is thus simply

$$-\Delta_{uv}\psi = E\psi, \tag{6}$$

where E is the eigenvalue of the eigenfunction ψ. As has been explained, we shall solve (6) on the unit disc (in the x, y plane) instead. The Laplace operator is thus conformally mapped,

$$\Delta_{uv} = \Delta_{xy}/J = (\partial^2/\partial x^2 + \partial^2/\partial y^2)/J, \tag{7}$$

where

$$J = |\mathrm{d}w/\mathrm{d}z|^2 = A^2(1 + 4\lambda^2 r^2 + 4\lambda r \cos\theta). \tag{8}$$

(Henceforth we shall drop the indices, i.e. $\Delta = \Delta_{xy}$.) Here, r and θ are the polar coordinates in the x, y plane. By inserting (7) into (6) we have

$$\Delta\psi + EJ(r, \theta)\psi = 0, \tag{9}$$

where Δ in polar coordinates is equal to

$$\Delta = \partial^2/\partial r^2 + r^{-2}\,\partial^2/\partial\theta^2. \tag{10}$$

Suppose the set $\{\varphi_j\}$ of eigenfunctions of $-\Delta$ on the unit disc forms an orthonomal

basis. Let us expand our solution ψ,

$$\psi = \sum_j c_j \varphi_j. \tag{11}$$

Then it follows that

$$\sum_i c_i (z_i^2 \delta_{ij} - E J_{ij}) = 0, \tag{12}$$

where z_j^2 is the eigenvalue of $-\Delta$ corresponding to the eigenfunction φ_j, and

$$J_{ij} = \langle \varphi_i | J | \varphi_j \rangle = (\mathsf{J})_{ij} \tag{13}$$

are the elements of the matrix J. By the definition of the matrix U,

$$(\mathsf{U}^{-1})_{ij} = z_i \delta_{ij}, \tag{14}$$

and the vector

$$(\boldsymbol{c})_i = c_i, \tag{15}$$

equation (12) appears in the compact form

$$(\mathsf{U}^{-1}\mathsf{1}\mathsf{U}^{-1} - E\mathsf{J})\boldsymbol{c} = 0. \tag{16}$$

Now, by multiplying by U from the left and defining $\mathsf{U}^{-1}\mathsf{c} = \boldsymbol{k}$ we obtain

$$(E^{-1}\mathsf{1} - \mathsf{UJU})\boldsymbol{k} = 0. \tag{17}$$

The eigenvalues E are obtained from the solutions of the secular equation

$$\det|\mu \mathsf{1} - \mathsf{UJU}| = 0, \tag{18}$$

where $E = 1/\mu$, and $\boldsymbol{c} = \mathsf{U}\boldsymbol{k}$, with $\boldsymbol{k}$ being the corresponding eigenvector of the matrix UJU.

Our numerical method is the diagonalisation of the matrix UJU in a truncated basis $\{\varphi_i\}$, $1 \leq i \leq N$. Let us determine the basis $\{\varphi_i\}$. The eigenfunctions of (10) are the products of Bessel and trigonometric functions,

$$\varphi_{k,n} = R_{k,n} J_k(\gamma_{k,n} r) \begin{Bmatrix} \cos k\theta \\ \sin k\theta \end{Bmatrix}, \tag{19}$$

with the normalisation constants

$$R_{0,n} = [\sqrt{\pi} J_0'(\gamma_{0,n})]^{-1}, \qquad R_{k,n} = [\sqrt{2}/\sqrt{\pi} J_k'(\gamma_{k,n})], \qquad k > 0. \tag{20}$$

Here J_k is the Bessel function of order k, $\gamma_{k,n}$ is its nth zero, and J_k' is the derivative of J_k. The eigenvalue of the Laplace operator (10) corresponding to a basis function (19) is given by

$$-\Delta \varphi_{k,n} = \gamma_{k,n}^2 \varphi_{k,n}. \tag{21}$$

When the eigenfunctions $\varphi_{k,n}$ are rearranged in order of increasing eigenvalues $\gamma_{k,n}^2$, we define a map $(k, n) \mapsto i = i(k, n)$ (and the inverse map $k = k(i)$, $n = n(i)$). For the lowest levels this map is reproduced in table 1. Then $z_i = \gamma_{k(i),n(i)}$, and $(\mathsf{U})_i = 1/z_i$ (see equation (14)).

In order to work out the diagonalisation procedure (17) we need to calculate the matrix elements J_{ij} of J (equation (13)). From (8) we have

$$J_{ij} = A^2(\delta_{ij} + 4\lambda^2 \langle \varphi_i | r^2 | \varphi_j \rangle + 4\lambda \langle \varphi_i | r \cos\theta | \varphi_j \rangle). \tag{22}$$

Table 1. The ordering mapping of the zeros $\gamma_{k,n}$ of the Bessel functions according to the increasing value.

i	k	n	i	k	n
1	0	1	26	2	4
2	1	1	27	7	2
3	2	1	28	0	5
4	0	2	29	11	1
5	3	1	30	5	3
6	1	2	31	8	2
7	4	1	32	3	4
8	2	2	33	1	5
9	0	3	34	12	1
10	5	1	35	6	3
11	3	2	36	9	2
12	6	1	37	4	4
13	1	3	38	13	1
14	4	2	39	2	5
15	7	1	40	0	6
16	2	3	41	7	3
17	0	4	42	10	2
18	8	1	43	14	2
19	5	2	44	5	4
20	3	3	45	3	5
21	1	4	46	8	3
22	9	1	47	1	6
23	6	2	48	11	2
24	4	3	49	15	1
25	10	1	50	6	4

It is seen here that $\langle\varphi_i|r^2|\varphi_j\rangle$ and $\langle\varphi_i|r\cos\theta|\varphi_j\rangle$ vanish if $\varphi_i \propto \cos k\theta$ and $\varphi_j \propto \sin k\theta$. In other words, our perturbation of the unit disc preserves the mirror symmetry (parity) with respect to the horizontal axis. This is immediately clear by looking at figure 1. In order to study the generic spectral properties it is necessary to eliminate all exact symmetries. Therefore, in the following we shall restrict ourselves to the study of states with positive parity, i.e. those states ψ that are linear combinations of $\cos k\theta$, $k = 0, 1, 2, \ldots$. Our basis functions are then nondegenerate and ordered according to increasing eigenvalues as described above.

The matrix elements of (22) are given by the integrals

$$\langle k'n'|r^2|kn\rangle = f\delta_{k'k}R_{kn}R_{k'n'}\int_0^1 \mathrm{d}r\, r^3 J_{k'}(\gamma_{k',n'}r)J_k(\gamma_{k,n}r),$$

where

$$f = \begin{cases} 2\pi, & k = 0, \\ \pi, & k > 0, \end{cases} \tag{23}$$

and

$$\langle k'n'|r\cos\theta|kn\rangle = g_{k'k}R_{k'n'}R_{kn}\int_0^1 \mathrm{d}r\, r^2 J_{k'}(\gamma_{k',n'}r)J_k(\gamma_{k,n}r),$$

where

$$g_{k'k}=\begin{cases}\pi, & k'=0,\ k=1 \text{ or } k=1,\ k'=0,\\ \pi/2, & k'=k\pm 1,\ k'\neq 0,\ k\neq 0,\\ 0, & \text{otherwise.}\end{cases} \tag{24}$$

Notice the very important circumstance that the parameter dependence of the matrix J is known, since the integrals (23)–(24) play the role of constants and must be calculated only once. This distinguishes our system from others, where the integration must be repeated for each new value of a parameter. Since it is just the integration that is most expensive, the separation of the parameter dependence is an extremely important property of our problem. For example, all calculations have been done on the Cyber 176 computer in double precision (28 decimal places working precision; but the actual accuracy in calculating and integrating the Bessel functions was 20 digits). The integrations were carried out for a 310×310 matrix. In this case there are 8956 nonvanishing integrals. The required computer time was about 10 hours. But the diagonalisation of a 150×150 matrix requires only 50 seconds computer time, so that the eigenvalue problem was easily solved for 400 parameter values p, which is enough to obtain a smooth variation of the eigenvalues with p.

As concerns the numerical procedure we have checked the accuracy of integration (Gaussian integration with twice 32 nodes) by using the orthogonality property of the Bessel functions. At least 20 figures were found correct. Further, when diagonalising we have taken $N=100$ and then also $N=150$. The convergence of levels was inspected: the ground level was accurate to eight decimal places, the 40th level to four places and the 70th level to two places. The analysis of the results presented in this work is restricted to the lowest 40 levels, whose relative accuracy is at least 10^{-4} or slightly better, except for figure 2 where 70 levels are plotted—because the numerical error is still less than the plot error.

4. The spectrum

In figure 2 we show the lowest 70 levels as functions of p, $0\leqslant p\leqslant p_{\text{sing}}$. For small $p\geqslant 0$, k and n are good quantum numbers, and their values can be read off in table 1. We see that the levels are on the average straight horizontal lines. In other words, the number of levels below the given energy (the so-called mode number) does not change very much with p because the area of the billiard is constant (Weyl area formula, Thomas–Fermi rule). More precise prediction of the mode number $N(E)$ as a function of energy is obtained by applying the generalised Weyl asymptotic formula (Baltes and Hilf 1978),

$$N(E)=\frac{\mathscr{A}E}{4\pi}-\frac{\mathscr{L}\sqrt{E}}{4\pi}+\frac{1}{12\pi}\oint\mathscr{K}(s)\,\mathrm{d}s+\sum_{\text{corners}}\frac{\pi^2-\alpha_i^2}{24\pi\alpha_i} \tag{25}$$

where $\mathscr{A}$ is the area, $\mathscr{L}$ the perimeter, $\mathscr{K}(s)$ the curvature (positive when convex outwards) as a function of the arc length s, and α_i are the interior corner angles†. In our case $\mathscr{A}=\pi$, while the perimeter $\mathscr{L}$ is equal to the integral

$$\mathscr{L}=A\int_0^{2\pi}\mathrm{d}\theta\,(1+4\lambda^2+4\lambda\cos\theta)^{1/2}. \tag{26}$$

† Equation (25) is a consistent asymptotic expansion, containing all terms that do not vanish as the wavelength goes to zero.

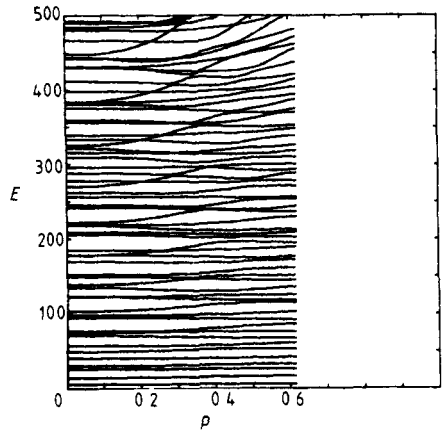

Figure 2. The spectrum (70 levels of even parity) for the billiard box as a function of the parameter p. The labels (k, n), which are good quantum numbers for small perturbations of the circular boundary, are given in table 1.

Since $A=(1+2\lambda^2)^{-1/2}$ we obtain the power expansion

$$\mathscr{L}=2\pi(1+\tfrac{3}{4}\lambda^4-\lambda^6+\ldots). \tag{27}$$

Next we calculate the curvature,

$$\mathscr{K}=(1+8\lambda^2+6\lambda\cos\theta)/(1+4\lambda^2+4\lambda\cos\theta)^{3/2}. \tag{28}$$

Its integral along the boundary,

$$\oint \mathscr{K}(s)\,\mathrm{d}s=\int_0^{2\pi}\mathrm{d}\theta\frac{1+8\lambda^2+6\lambda\cos\theta}{1+4\lambda^2+4\lambda\cos\theta}, \tag{29}$$

turns out to be independent of λ, namely

$$\oint \mathscr{K}(s)\,\mathrm{d}s=2\pi. \tag{30}$$

Inserting $\mathscr{A}=\pi$, (27) and (30) in the expression (25) yields the mode number $N(E,\lambda)$,

$$N(E,\lambda)=\tfrac{1}{4}E-\tfrac{1}{2}\sqrt{E}(1+\tfrac{3}{4}\lambda^4-\lambda^6+\ldots)+\tfrac{1}{6}. \tag{31}$$

This is the total number of modes, including even and odd parity. Our numerical calculations have been done for even parity, and to compare the results with the theory we have to subtract from (31) the number of modes of odd parity. The wavefunctions of odd parity are linear combinations of $\sin k\theta$, $k=1,2,3,\ldots$, so that they are the solutions of the eigenvalue problem on the desymmetrised billiard. This is bounded by the upper half of the curve (2) and by the x axis. Therefore,

$$\mathscr{A}_{\mathrm{odd}}=\pi/2, \qquad \mathscr{L}_{\mathrm{odd}}=\tfrac{1}{2}\mathscr{L}+2A=\tfrac{1}{2}\mathscr{L}+2/(1+2\lambda^2)^{1/2}, \tag{32}$$

$$\oint \mathscr{K}_{\mathrm{odd}}(s)\,\mathrm{d}s=\tfrac{1}{2}\oint \mathscr{K}(s)\,\mathrm{d}s=\pi,$$

and the corresponding mode number (with corner corrections included),

$$N_{\mathrm{odd}}(E,\lambda)=\tfrac{1}{8}E-\tfrac{1}{4}\mathscr{L}_{\mathrm{odd}}\sqrt{E}+\tfrac{5}{24}. \tag{33}$$

Consequently, $N_{\text{even}}(E,\lambda)=N(E,\lambda)-N_{\text{odd}}(E,\lambda)$ follows from (31)–(33):

$$N_{\text{even}}(E,\lambda)=\tfrac{1}{8}E-\tfrac{1}{2}\sqrt{E}[\tfrac{1}{2}-\pi^{-1}+\pi^{-1}\lambda^2-\tfrac{3}{2}(\pi^{-1}-\tfrac{1}{4})\lambda^4+\tfrac{1}{2}(5/\pi-1)\lambda^6+\ldots]-\tfrac{1}{24}. \quad (34)$$

Because $0\leqslant\lambda<\frac{1}{2}$ and since the lowest term of the power expansion in λ is quadratic, the dependence of $N_{\text{even}}(E,\lambda)$ on λ is indeed very weak. In figure 3 we compare the numerically calculated mode number for even states with the theoretical result $N_{\text{even}}(E,\lambda)$, as given in (34). The agreement is very good. The broken curves are the result of the Weyl area formula, and we see that the perimeter corrections according to (34) are significant. The mode number $N_{\text{even}}(E,\lambda)$ is almost independent of $\lambda=(1/\sqrt{2})\tan p$, as predicted by the theory.

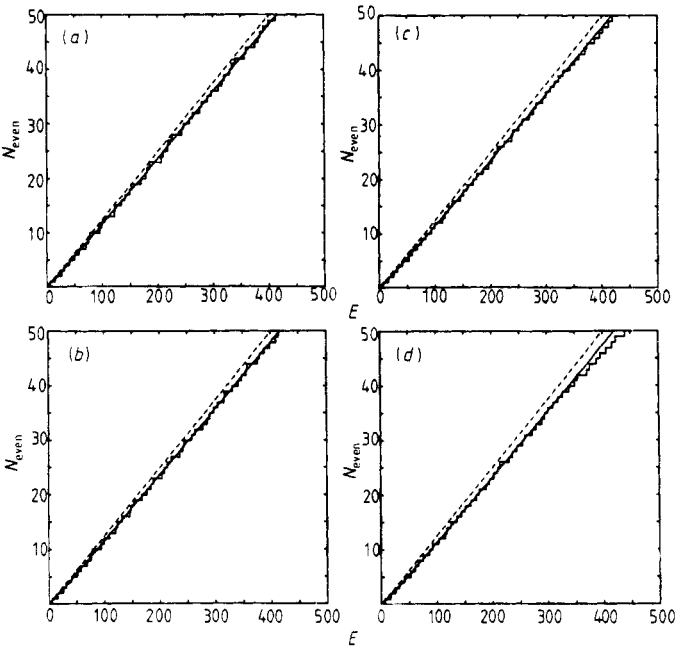

Figure 3. The mode number $N_{\text{even}}(E,\lambda)$ for even states as a function of energy, according to the numerical results. The prediction by the Weyl area formula (i.e. Thomas–Fermi rule) is represented by the broken curve, and is seen to be significantly improved by including the perimeter and curvature corrections (full curve) according to (34). The mode number $N_{\text{even}}(E,\lambda)$ varies only slightly with λ, as predicted by (34), and shown for (*a*) $p=0.1536$, (*b*) $p=0.3077$, (*c*) $p=0.4608$, (*d*) $p=p_{\text{sing}}=0.6155$.

Because the mode number is (almost) independent of p the mean level spacing is (almost) constant as well. The spectrum is thus surprisingly rigid. Even near the singular point $p=p_{\text{sing}}$ ($\lambda=\frac{1}{2}$), where a cusp of the boundary appears at $\theta=\pi$, there are no dramatic changes in the spectrum. There are, however, some levels with large positive slope (figure 2). The constancy of the mode number is maintained in that the number of ascending levels is approximately equal to the number of descending levels. They do not cross but participate in avoided crossings, where they are mutually repelled. In fact the levels exchange their approximate ('local') asymptotes. For instance, a horizontal almost constant level becomes steep and the steep one becomes almost constant. It will be seen in § 5, when we shall analyse the corresponding wavefunctions, that there is a kind of 'exchange of identity' between the states participating in an

avoided crossing. This is a consequence of the strong mixing of states near an avoided crossing. If the avoiding of levels is ignored as the lowest approximation, thereby pretending a level crossing, then the 'exchange of identity' explains why such a crude approximation is surprisingly fine (see also Ramaswamy and Marcus 1981).

In figure 4 we show the lowest levels on a finer scale. It should be observed that the ground level is (slightly) increasing. This agrees with a variational property of the circular disc: the ground eigenvalue of the negative Laplace operator on a plane region of constant area, with Dirichlet's boundary condition, is the lowest for a circular disc (Krahn 1925, Robnik 1980b). For any area preserving deformation of a circular disc, in particular for our billiard, the ground eigenvalue must increase.

In figure 5 we show the levels $(20 \leq i \leq 30)$ in the energy range $150 \leq E \leq 250$.

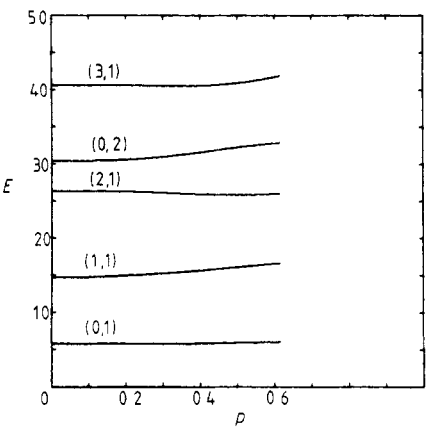

Figure 4. Five lowest levels of figure 2.

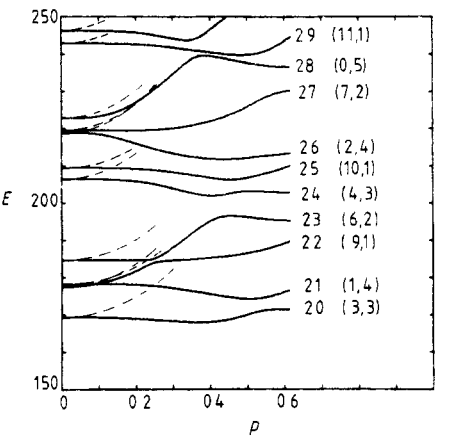

Figure 5. The levels E_i, $20 \leq i \leq 30$, in the energy range $150 \leq E_i \leq 250$. The lowest-order perturbation theory (according to (35) and shown by broken curves) yields best results for the levels $i = 21 (1, 4)$ and $i = 28 (0, 5)$, which correspond to the most stable classical tori for low p.

The broken lines are the results of the (lowest-order) perturbation theory, according to which

$$E(p) = E|_{p=0}(1 - \tfrac{1}{2}\tan^2 p\langle kn|r^2|kn\rangle)/\cos^2 p. \tag{35}$$

It is characteristic that some levels (e.g. $(k, n) = (1, 4)$ and $(0, 5)$ in figure 5) follow this prediction quite well for low p, while others do not. It can be shown that these 'surprisingly predictable' levels correspond to the most stable classical tori through the EBK quantisation (or better called, tori quantisation). Other features of the spectrum are better understood together with the wavefunctions in § 5.

Let us look at the semiclassical spectrum of the circular disc with radius equal to unity. As before we assume $\hbar^2/2m = 1$. The classical Hamilton function $H = \boldsymbol{p}^2$ corresponds to the quantum Hamiltonian $\hat{H} = \hat{p}^2 = -\Delta$. In polar coordinates the energy is equal to

$$E = p_r^2 + k^2/r^2, \tag{36}$$

where p_r is the radial momentum, and $k = 0, 1, 2, \ldots$ is the quantised value of the

angular momentum, which is a constant of the motion. Hence, the action

$$I_r = \frac{1}{2\pi}\oint p_r \, dr = \frac{1}{\pi}\int_{r_{min}}^{1} dr\left(E - \frac{k^2}{r^2}\right)^{1/2}, \tag{37}$$

where $r_{min} = k/\sqrt{E}$ is the radius of the circular caustic formed by the classical trajectories. The phase shift of the semiclassical wavefunction at the caustic is $\pi/2$, while at the reflecting boundary it is equal to π, because the wavefunction must vanish there. Consequently, the Maslov index α in the quantisation condition,

$$I_r = n - 1 + \alpha/4, \tag{38}$$

is equal to 3. Here $n = 1, 2, \ldots$, is the radial quantum number, i.e. $n-1$ is the number of nodes (excluding the boundary) of the radial wavefunction. From (37) and (38) we obtain the semiclassical energy levels $E_{k,n}$, given by

$$k \sin^{-1}(k/\sqrt{E_{k,n}}) + (E_{k,n} - k^2)^{1/2} = \pi(n - \tfrac{1}{4} + \tfrac{1}{2}k), \tag{39}$$

where the labelling is the same as in the exact solution $E_{k,n} = \gamma_{k,n}^2$ (equation (21)). The accuracy of the semiclassical approximation (39) is not excellent for low levels. For instance the ground level $E_{0,1} = (3\pi/4)^2 = 5.551\ldots$, while the exact value is $\gamma_{0,1}^2 = 5.783\ldots$. But the approximation becomes asymptotically better as $n \mapsto \infty$. In fact, the lowest term in the asymptotic expansion agrees with the exact expansion for the zeros of Bessel functions, namely

$$E_{k,n} = \pi^2(n - \tfrac{1}{4} + \tfrac{1}{2}k)^2[1 + O(1/n^2)], \tag{40}$$

but higher terms do not.

The numerical value of the semiclassical levels is not important in our context. We need the semiclassical picture for the identification of those classical tori and orbits on them which correspond to the exact eigenstates (19).

The association of the classical trajectories in configuration space with the quantum states follows from (39). We write the angular momentum k in the form

$$k = |\boldsymbol{p}| r_{min} = \sqrt{E} \sin \chi, \tag{41}$$

where χ is the reflection angle of the orbit (i.e. the angle between the velocity vector and the normal to the boundary, both pointing inwards). Hence, $\chi = 0$ (radial motion) for $k = 0$, while for $k \neq 0$ one has

$$\chi + \cot \chi = [(n - \tfrac{1}{4})/k + \tfrac{1}{2}]. \tag{42}$$

The above formula assigns classical orbits (specified by the angle of incidence χ) to the given exact quantum state (specified by the quantum numbers k and n). For example, for small n and large k the exact wavefunction (19) is concentrated near the boundary (because we have Bessel functions of high order), and is modulated by the high frequency angular dependence. This corresponds to the classical orbits with little radial motion (low n) and large angular momentum k. The classical motion is thus localised on a narrow circular annulus between the caustic and the boundary of the disc. This means $\chi \approx \pi/2$, in agreement with (42).

When this correspondence between the classical motion and quantum states is combined with the adiabatic picture, we are able to understand the qualitative properties of the spectrum and of the wavefunctions. We describe now this heuristic approach.

According to the adiabatic theorem of quantum mechanics (Landau and Lifshitz 1975) a system remains in the same state, following the continuously varying energy level, when a parameter of the Hamiltonian is (infinitely) slowly changing. In our case, with p varying, the system follows a given level $E_i(p)$. Consider a level with large positive slope. (For example $i = 28$, i.e. $(k, n) = (0, 5)$ shown in figure 5.) By increasing p we have to do work in order that the system is able to follow the increasing level $E_i(p)$. Classically, we do work against the 'pressure' of the colliding particle. But because our deformation is area preserving, this work is positive if the collisions appear predominantly in those regions where the boundary is moving inward with p increasing (compression). This implies that the corresponding classical orbits must be localised near the horizontal symmetry axis, because at $\theta = 0$ and $\theta = \pi$ the compression takes place (the distance between these points decreases as $2A = 2\cos p$). Therefore, we expect the corresponding exact wavefunction to be localised along the symmetry axis as well. This is indeed observed, and shown in § 6 (figure 10(*e*)).

Similar arguments explain the localisation of wavefunctions in the vertical direction (because of the expansion) for those quantum states with large negative slope ($\mathrm{d}E_i/\mathrm{d}p < 0$) of the corresponding level.

Finally, an energy level $E_i(p)$ is approximately constant ($\mathrm{d}E_i/\mathrm{d}p \approx 0$) if the corresponding wavefunction is isotropic either in an ordered manner (rotational symmetry), or in a random disordered manner (chaotic, highly mixed states). In the former case the classical motion is localised near the boundary (glancing trajectories), while in the latter case the classical motion is chaotic, e.g. ergodic. In both cases no or little work is done under a small and slow area preserving deformation.

We may formulate the qualitative relationship:

steep energy level ($|\mathrm{d}E_i/\mathrm{d}p| > 0$) $\leftrightarrow$ localised wavefunction ψ_i,

almost constant energy level ($\mathrm{d}E_i/\mathrm{d}p \approx 0$)
$\leftrightarrow$ isotropic wavefunction ψ_i (either ordered or disordered).

In the semiclassical picture the localisation of a quantum state corresponds to the localised classical motion in configuration space. The latter is a consequence of the existence of invariant tori. But then the associated actions are invariant, adiabatically (Whiteman 1977, Arnold 1980), i.e.

$$I = (2\pi)^{-1} \oint \boldsymbol{p} \cdot \mathrm{d}\boldsymbol{r} = \text{constant}.$$

This implies an approximate scaling law $E_i \propto 1/L^2$, where L is a typical length scale of the corresponding motion. For example, if $k = 0$, then $L = A$ and we have roughly $E_i \propto 1/\cos^2 p$, which agrees with the comparison of the perturbation theory with exact levels (figure 5): for the states $k = 0$ and $k = 1$, which are localised near the horizontal symmetry axis and correspond to the invariant tori around the stable period-two orbit, the agreement is the best. These are precisely those states with the smallest $\langle kn|r^2|kn\rangle$ (see (35)), so that they follow the above scaling rule quite well. Another example is the level $(k, n) = (10, 1)$, which corresponds to a glancing motion near the boundary. Here we may take $L \sim \mathscr{L}$. But the perimeter $\mathscr{L}$ of our billiard changes much more slowly with p than A. (See the power expansion (26).) Therefore the corresponding level should (and does) vary much more slowly than in the case $k = 0$.

On the other hand, having a chaotic classical motion, the adiabatic invariant is the phase space volume. The area preserving property of the deformation implies then

the constancy of energy. The corresponding quantum energy level is thus also expected to be almost constant. This is clearly seen in figure 2 for almost all states for the parameter values near $p \lesssim p_{\text{sing}}$. The classical system is highly chaotic there, as shown in (I).

5. The wavefunctions

In this section we describe the properties of eigenfunctions, and begin with the discussion of low states. Some of the corresponding levels are shown in figure 4. First of all, it has been verified that the ground state is nodeless for all p, as predicted by a general theorem (Courant and Hilbert 1968).

Low states are generally insensitive to the perturbations, as has been emphasised in the introduction (vii). This is explained by the large wavelengths of the standing waves: the wavefunction cannot 'see' the finest details of the boundary. In figure 6 we show the nodal pattern of the (0, 2) state in a circular disc (figure 6(a)), and we show how it changes (figures 6(b)–(d)) with the deformation of the boundary. There are no dramatic changes. For example, it is conceivable that a nodal cell (e.g. the black inner disc) would become not only stretched, but would also wind in a turbulent,

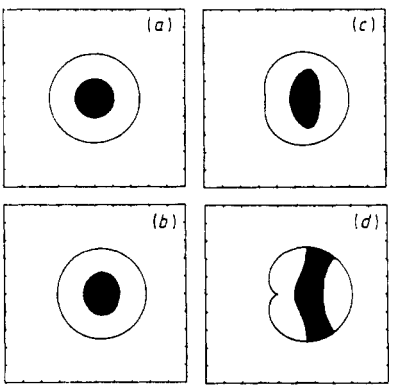

Figure 6. The nodal structure of the wavefunction ψ_4 as a function of p, (a) $p=0$, (b) $p=0.2$, (c) $p=0.4$, (d) $p=p_{\text{sing}}=0.6155$. At low $p \to 0$, ψ_4 is labelled by $(k, n)=(0, 2)$ (see (19)). The units are the same for both coordinates, but otherwise arbitrary.

mixing way. In addition, it is also conceivable that new, arbitrary small nodal cells appear, split and disappear. All this is not observed. There is an explanation for the absence of such mixing and splitting properties: there exists a lower bound for the area of a nodal cell (Robnik 1980a). This is discussed in the appendix. In our two-dimensional case the lower bound $\mathscr{A}_{\min}$ is given by

$$\mathscr{A}_{\min} = \pi \gamma_{0,1}^2 / E, \tag{43}$$

where E is the energy eigenvalue of the state. The area of the black region in figure 6(a) reaches the lower bound (43), because it has a circular shape. Indeed, since $E_4 = \gamma_{0,2}^2$, the radius $r_b = \gamma_{0,1}/\gamma_{0,2}$ inferred from (43) agrees with the nodal radius of the exact wavefunction $\varphi_{0,2} \propto J_0(\gamma_{0,2} r)$. As p varies, the energy level $E_4(p)$ increases slightly, as shown in figure 4. The lower bound $\mathscr{A}_{\min}$ decreases—but only slightly. Consequently,

the black nodal cell cannot be split into two cells with p varying. The white cell, which is a circular annulus at $p=0$ and the area of which is greater than $2\mathscr{A}_{\min}$, can be split into two cells. This is actually observed in figure 6(d). But further splitting of cells is forbidden.

A rough estimate of the upper bound $\mathscr{L}_{\max}$ of the perimeter of a nodal cell is obtained from the generalised asymptotic formula (25), by ignoring the constant term, and by requiring $N(E)>0$, whence

$$\mathscr{L}_{\max} \cong \mathscr{A}\sqrt{E} \leqslant \pi E.$$

We can thus understand why there cannot be an arbitrary number of cells in the nodal pattern, provided the energy is bounded. We can also understand that the nodal cells cannot be stretched (to form a thin ribbon), and cannot be mixed arbitrarily: this would imply a large increase of the eigenvalue, determined roughly by a typical length scale of the ribbon, namely by its thickness. As the (mean) thickness went to zero the energy would go to infinity.

The variation of the nodal structure shown in figure 6 is a counterexample to a claim on the adiabatic invariance of the number of nodal cells (Robnik 1980a). The latter was based on misleading topological arguments, and I have criticised that already (Robnik 1981). Korsch (1983) has recently reviewed the generic properties of nodal structure, and his compilation will be useful in the discussion of higher states, below. However, he does not mention the important property on the lower bound for the area of nodal cells, which we discuss in the appendix. (A weaker property is well known (Courant and Hilbert 1968): the nth state cannot have more than n nodal cells. But this says nothing about the size of the cells.)

Now we are going to study higher states, corresponding to the levels in figure 5. Consider first the level $i=23$, whose label at small p is (6, 2). It is almost constant until it collides with the level $i=22$ in the avoided crossing near $p=0.25$. Its approximate constancy implies—as argued in § 4—that the wavefunction is either localised in an ordered manner, with rotational symmetry, or chaotic. In figures 7(a)–(f) we show

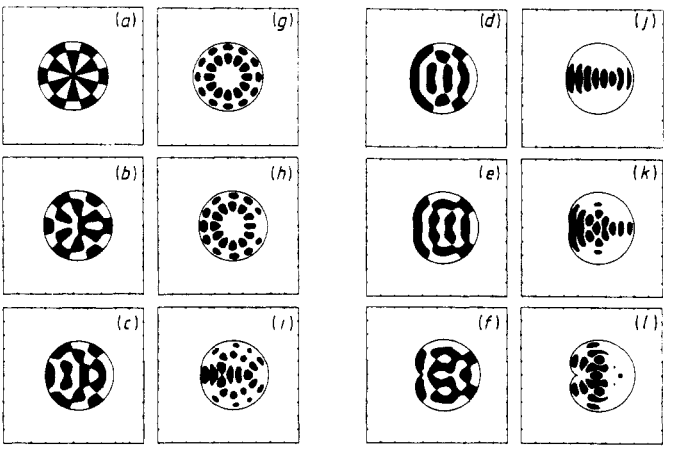

Figure 7. The nodal structure of the wavefunction ψ_{23} as a function of p, (a) $p=0$, (b) $p=0.2$, (c) $p=0.25$, (d) $p=0.3$, (e) $p=0.4$ and (f) $p=p_{\text{sing}}=0.6155$. For the same set of the parameter values we show the localisation properties of the wavefunction (g, l). In black regions the probability density ψ_{23}^2 exceeds its average value $1/\pi$ (arbitrary units).

how the nodal pattern changes with p, while in figures 7(g)–(l) we plot in black the regions where the probability density ψ_{23}^2 is larger than its mean value $1/\pi$. It is seen, indeed, that the state is localised on a circular annulus at small p, and becomes chaotic near the avoided crossing at $p \approx 0.25$, as shown in figure 7(i). This a consequence of the mixing of states $i = 23$ and $i = 22$. At the avoided crossing these states exchange their identity, and the level $E_{23}(p)$ becomes a steep function of p. As argued in § 4, this implies a localisation of the probability density near the horizontal symmetry line, which is actually observed for $p = 0.3$ in figure 7(j). Near $p \approx 0.4$ a distant repulsion by the upper level ($i = 24$) appears, and $E_{23}(p)$ becomes weakly decreasing. Again, using the heuristic arguments within the adiabatic picture, we understand that the state is now (weakly) localised in the vertical direction, as shown in figure 7(l).

Using this example we would like to emphasise that classical chaos does not necessarily imply quantum chaos, as pointed out by Noid *et al* (1980). More precisely, at $p = 0.3$ there exist almost no classical tori, and the system is largely chaotic (I). Nevertheless, in figure 7(j) we have a clear example of a localised, non-random state.

As seen in figure 5 the level $E_{25}(p)$ is almost constant. Because $k = 10$, $n = 1$ the state is localised near the boundary, at small p (figure 8). This is consistent with the (approximate) constancy of the level. Near $p \approx 0.4$ (figure 8(g)) the inner boundary of the localisation region is deformed in a manner that reminds us of the deformation of classical caustics (I). But again, one should not forget that at $p = 0.4$ no classical tori and caustics exist. This is thus again an example that a straightforward analogy between the classical and quantum chaos runs into difficulties. It seems that quantum localisation properties ('quantum tori') persist far beyond the classical stochasticity

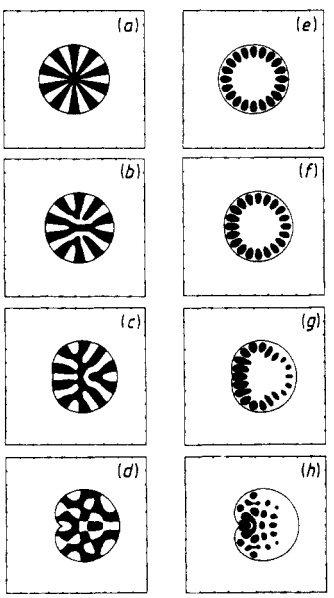

Figure 8. The nodal structure of the wavefunction ψ_{25} as a function of p, (a) $p = 0$, (b) $p = 0.2$, (c) $p = 0.4$, (d) $p = p_{\text{sing}} = 0.6155$. At the same values of p we show the domains (in black) where the probability density is larger than its mean value $1/\pi$ (e)–(h) (arbitrary units).

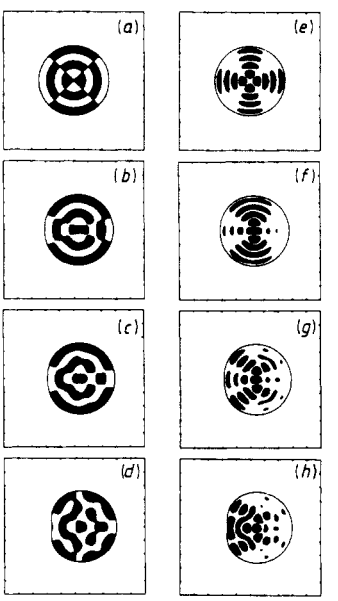

Figure 9. The same as figure 8, but for the wavefunction ψ_{26}, and $p = 0$, 0.2, 0.3 and 0.4.

threshold (cf Noid *et al* 1980). A classical analogue may be a long-lived transient (but not asymptotic) localisation of trajectories, which undergo a slow diffusion near the remnants (i.e. small stability islands) of a broken torus. Such a phenomenon has been observed in the classical dynamics of our billiard (I), but not at the parameters of the specific example above. Jaffé and Reinhardt (1982) have recently studied transient dynamical behaviour of the Hénon–Heiles system. They demonstrate regularity on short to intermediate time scales, resulting in a transient confinement of orbits to vague tori (Shirts and Reinhardt 1982), which seems to be useful for semiclassical quantisation. This is an important link between the dynamical and the structural point of view. It shows that the asymptotic structure of the classical phase space may not be enough to deduce the quantum mechanical structure, but the time dependent structure might be essential, instead. Of course, the latter is identical to the asymptotic structure only in integrable cases. In the specific example of the level $i=25$ near $p=0.4$ we have not found any transient behaviour of such type.

Next we analyse the level $i=26$, which is approximately constant at $p \leqslant 0.1$. The corresponding eigenfunction (figure 9(*a*, *e*)) has two localisation regions, a vertical and a horizontal. The existence of the former would imply a positive derivative dE_{26}/dp, while the latter implies $dE_{26}/dp < 0$. The two contributions compensate for each other, resulting in an approximate constancy of the eigenvalue. At $p \geqslant 0.2$ the energy is decreasing, until $p \approx 0.4$. Therefore, the state is localised mainly along a vertical elongated region. For $p \geqslant 0.4$ the energy is again almost constant, and the state is largely chaotic, but nevertheless concentrated in the left side of the box (figure 9(*h*)).

In the next example of the level $i=28$, which is a rapidly increasing function of p until it eventually collides with the level $i=29$ near $p \approx 0.35$, we demonstrate a spectacular localisation of the corresponding state—as a consequence of the symmetry breaking. In figure 10(*d*) the state is rotationally symmetric and fills the whole box

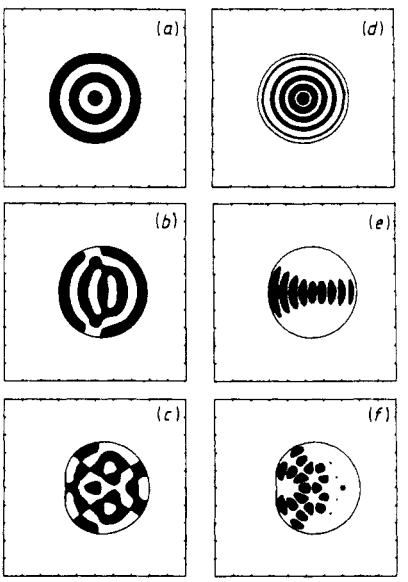

Figure 10. The nodal pattern of the wavefunction ψ_{28} as a function of p, (*a*) $p=0$, (*b*) $p=0.25$ and (*c*) $p=0.4$. In (*d*)–(*f*) we show the localisation properties for these states, respectively. The black regions are domains where the probability density ψ_{28}^2 exceeds its average value $1/\pi$.

rather uniformly. As a result of the symmetry breaking of the circular disc, the wavefunction becomes strongly localised on a domain elongated along the symmetry line. This must be so if the level $E_{28}(p)$ should increase rapidly. However, at $p \approx 0.4$ the level has a much smaller slope and the state becomes delocalised.

We can conclude that mixing of states occurs at avoided crossings, which implies a randomised wavefunction. An example *par excellence* of such mixing is the avoided crossing between the levels $i=22$ and $i=23$ near $p=0.25$. Figures $7(h, i, j)$ are a clear demonstration. Classical chaos by itself does not imply a particular chaotic quantum state, and *vice versa*. By a chaotic quantum state we mean one such that the wavefunction is *not* localised, has a random appearance, and the probability density is determined by the ergodic average over the energy surface, projected onto configuration space. It appears that classical chaos does imply quantum chaos in the statistical sense, i.e. it implies enhanced probability for avoided crossings. Therefore, with the onset of classical stochasticity the number of chaotic quantum states increases.

6. The statistical properties of the spectrum

It has been predicted (Zaslavsky 1977, 1979, 1981, Berry 1977a, b, 1981, 1983a, Berry and Tabor 1977) that a drastic change in the distribution of spacings between adjacent levels accompanies the transition from an integrable to a nonintegrable case. Let $P(S)\,\mathrm{d}S$ be the probability that a spacing S (in units of the mean level spacing) lies between S and $S+\mathrm{d}S$. Then $P(S)=\mathrm{e}^{-S}$ (Poisson distribution) in integrable systems, while in chaotic systems one expects $P(S)=\text{constant}\times S^{\nu}$ for small S. There is a disagreement about the critical exponent ν, as it might be called. Berry's geometrical derivation (Berry 1981, 1983a) predicts $\nu=1$ (Wigner distribution). By using a semiclassical approach Zaslavsky derives a relation between the critical exponent ν and the Kolmogorov entropy h of the corresponding classical system, namely

$$\nu = \text{constant}/T_0 h - 1, \tag{44}$$

where T_0 is the period of the closed orbits near the maximum of their distribution. (Zaslavsky absorbs T_0 in h to make h dimensionless entropy.) This derivation is valid only for sufficiently chaotic systems (due to the arguments he uses), so that the limit of integrable systems ($h \to 0$) may not be taken in (44).

The most important qualitative feature shared by both predictions is the phenomenon of the level repulsion: as $S \to 0$, then $P(S)=\text{constant}\times S^{\nu} \to 0$ if ν is positive. This is related to the fact that level crossings are forbidden in nonintegrable systems (Von Neumann and Wigner 1929), and avoided crossings appear instead. This is in contrast to the existence of level crossings in integrable systems. In the latter case the levels are uncorrelated and therefore Poisson distributed. In the former case there is a correlation between the levels—because of the repulsion—and they can be neither Poisson nor Gaussian distributed, because $P(S)$ must vanish as $S \to 0$.

McDonald and Kaufman (1979) presented the level spacing distributions for a circular disc (integrable) and for the stadium (nonintegrable). The transition from the Poisson distribution to a distribution similar to the Wigner distribution is clearly seen there, notably the drop of $P(S)$ near $S=0$. In spite of the importance of this problem there is still no convincing quantitative test of various predictions. The reason is that it is extremely difficult to calculate a large enough number N of levels to overcome the $1/\sqrt{N}$-fluctuations in the statistics and to make definite conclusions about the

critical exponent ν, since one needs a high resolution of histogram at small S. How can we overcome this difficulty?

The answer is that there are robust properties of the distribution $P(S)$, which are relatively easy to measure—to the crudest approximation, at least. When reviewing the random matrix mechanics Brody *et al* (1981) give the following derivation due originally to Wigner (1967). Consider the equation

$$P(S)\,\mathrm{d}S = W(1 \in \mathrm{d}S | 0 \in S)\, W(0 \in S), \tag{45}$$

saying that the probability of finding a level within $\mathrm{d}S$ near S is equal to the conditional probability,

$$r_{10}(S)\,\mathrm{d}S := W(1 \in \mathrm{d}S | 0 \in S), \tag{46}$$

of having a level within $\mathrm{d}S$ at S but none within S, times the probability of having no level within S,

$$W(0 \in S) = \int_S^\infty P(x)\,\mathrm{d}x. \tag{47}$$

Hence,

$$P(S) = r_{10}(S) \int_S^\infty P(x)\,\mathrm{d}x, \tag{48}$$

which can be easily solved for P to yield

$$P(S) = \text{constant} \times r_{10}(S) \exp\left(-\int^S r_{10}(x)\,\mathrm{d}x\right). \tag{49}$$

The 'law of level repulsion' described by the probability density $r_{10}(S)$ is still arbitrary. The importance of the result (49) is that it predicts an overall change of $P(S)$ when $r_{10}(S)$ is varied.

Let us assume a power law for the repulsion of levels,

$$r_{10}(S) = \text{constant} \times S^\nu, \tag{50}$$

where ν is the critical exponent. By inserting this into (49) we have still two arbitrary constants a and b,

$$P(S) = aS^\nu \exp(-bS^{\nu+1}), \tag{51}$$

which are determined by two conditions, the normalisation of $P(S)$,

$$\int_0^\infty P(x)\,\mathrm{d}x = 1, \tag{52}$$

and the normalisation of the first moment, which is equal to 1 by definition,

$$\int_0^\infty xP(x)\,\mathrm{d}x = 1. \tag{53}$$

It follows then that

$$a = (\nu+1)\left[\Gamma\left(\frac{1}{\nu+1}+1\right)\right]^{\nu+1}, \qquad b = \frac{a}{\nu+1} = \left[\Gamma\left(\frac{1}{\nu+1}+1\right)\right]^{\nu+1}. \tag{54}$$

where $\Gamma(x)$ is the gamma function.

The robust quantity we meant before is the dispersion of $P(S)$, for instance. This is given by

$$\sigma^2 = \langle S^2 \rangle - 1 = \int_0^\infty x^2 P(x)\,\mathrm{d}x - 1, \tag{55}$$

and by using (51) and (54) we find that it is a decreasing function of the exponent ν,

$$\sigma^2 = 2(\nu+1)\Gamma(2/(\nu+1))/[\Gamma(1/(\nu+1))]^2 - 1. \tag{56}$$

Therefore, by measuring σ we can determine ν. The dispersion σ as a function of ν according to the above equation is shown in figure 11. In particular, we notice that for $\nu = 0, 1$ we obtain Poisson and Wigner distributions, respectively.

Poisson ($\nu = 0$):

$$P(S) = \mathrm{e}^{-S}, \qquad \sigma = 1.$$

Wigner ($\nu = 1$):

$$P(S) = \tfrac{1}{2}\pi S \exp(-\tfrac{1}{4}\pi S^2), \qquad \sigma = (4/\pi - 1)^{1/2}.$$

Zaslavsky predicts also other cases, according to the continuous variation of ν with h (equation (44)). As the entropy h increases, the critical exponent ν decreases, which in turn predicts a spreading of the distribution $P(S)$, i.e. an increasing σ. In our numerical results (figure 12) we observe the opposite. We plot normalised histograms in eight parameter intervals of equal size, each containing 50 parameter values p, and at each p we have taken the lowest 40 levels (accurate to four decimal places). Hence, for each histogram we have used 2000 levels. The dispersion σ decreases gradually as p_0 ($p = p_0$ is the centre of the parameter interval for which a histogram is shown) increases, while Zaslavsky's relation would predict the opposite, because the K entropy increases with p, as has been calculated in (I). There may be several reasons for this discrepancy. (i) The statistics are still too bad (although it is very unlikely that they

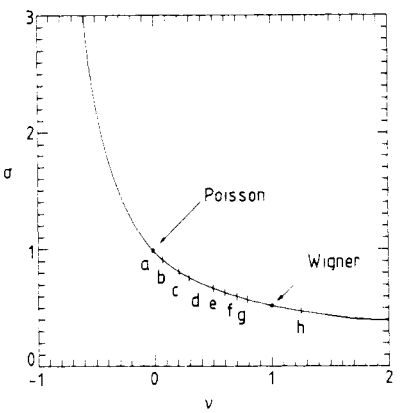

Figure 11. The dispersion $\sigma(\nu)$ as a function of the critical exponent ν as given by (56). The Poisson and Wigner distributions correspond to the points $\nu = 0$, $\sigma = 1$ and $\nu = 1$, $\sigma = (4/\pi - 1)^{1/2}$, respectively. We show also the values of σ as calculated for the histograms of figure 12, and given in table 2. A transition from the Poisson to the Wigner distribution with increasing σ is clearly seen. Note that the Kolmogorov entropy increases with p very rapidly (I), as shown in table 2.

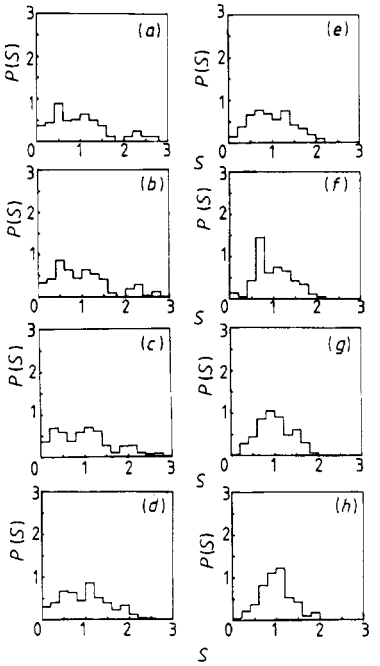

Figure 12. Histograms for the level spacing distribution at various p_0. (*a*) $p_0 = 0.04$, (*b*) $p_0 = 0.12$, (*c*) $p_0 = 0.19$, (*d*) $p_0 = 0.27$, (*e*) $p_0 = 0.35$, (*f*) $p_0 = 0.42$, (*g*) $p_0 = 0.50$, (*h*) $p_0 = 0.58$. In each histogram p_0 is the centre of an interval of size $\Delta p = 0.077$. In each interval the spectrum has been calculated for 50 equidistant parameter values p, and for each p the lowest 40 levels, accurate to four places, have been included. Hence, each histogram contains 2000 level spacings. The histograms are normalised according to (52)–(53). A gradual transition from the Poisson distribution ($\sigma = 1$) to the Wigner distribution ($\sigma = (4/\pi - 1)^{1/2}$) is seen. The calculated σ's and the inferred ν's are shown in figure 11 and their values are listed in table 2.

yield such strongly distorted qualitative features, because $1/\sqrt{N} \approx 0.02$). (ii) The 40 levels we use might be too low to lie in the semiclassical region, which which Zaslavsky's result is supposed to be valid. (iii) The assumption $r_{10} \propto S^{\nu}$ in the heuristic derivation by Wigner (1967), as given by (45)–(48), is not realistic. (We comment on this below.) (iv) The relation (44) fails for some reason, or else Zaslavsky's prediction refers to the fine structure ($S \to 0$) that we are not able to resolve.

The reason (i) can be almost excluded. The second comment (ii) might be the truth, but it would be very surprising if the low levels behave in a completely different manner from the higher levels, where the semiclassical picture is valid. As concerns Wigner's derivation, Brody *et al* (1981) pointed out two difficulties. The first question was the hypothesis of the linear repulsion ($r_{10}(S) \propto S$), which we have relaxed already. The second problem is more serious: $r_{10}(S) = \text{constant} \times S^{\nu}$ increases as $S \to \infty$, and is thus certainly wrong for large S, but is most probably correct for small S. In fact $r_{10}(S)$ must vanish when S goes to infinity. There is thus an open question of how to determine a correct $r_{10}(S)$, which we are not going to solve. Our conclusions on ν are based on the ansatz (51) and on the derived relation $\sigma(\nu)$ in (56), and are thus indirectly subject to the Wigner-like surmise (50).

As concerns the applicability of the relation (44) we are not able to present any serious objection to Zaslavsky's derivation. The objection of taking the almost periodic

orbits, raised by Berry (1981, 1983a), is not justified in our opinion (Robnik and Zaslavsky 1983). The point is that the statistical properties of semiclassical spectra are determined by the statistical properties of strictly periodic orbits. But these properties do not change if we consider almost periodic orbits instead. If they changed in a drastic manner, then by reasons of structural stability with respect to discretisation the periodic orbits would have no meaning for the spectrum—which is refused by everybody.

Now, it should be emphasised that the histograms in figure 12 do show clear evidence for a decreasing dispersion σ as the system goes from the integrable ($p=0$) to the nonintegrable case ($p \leqslant p_{\text{sing}}$). This means a trend from the Poisson distribution to the Wigner distribution, as shown in figure 11. But notice the fact that this variation is a gradual (continuous) one. We do not believe that this is an artifact of bad statistics, as argued in (i) above. But then, taking this phenomenon seriously (in a qualitative sense), we have problems with the geometrical derivation by Berry (1981, 1983a) as well. According to his prediction one would always expect the Wigner distribution, no matter how large the degree of nonintegrability and chaos†. (This is true for real Hermitian matrices—as is the case in our problem of quantising the billiard. For complex Hermitian matrices he predicts $\nu=2$.) Hence, one would expect a discontinuous transition from $\nu=0$, $\sigma=1$ (Poisson) to $\nu=1$, $\sigma=(4/\pi-1)^{1/2}$ (Wigner), and σ should thus be constant for all $p>0$. This is not observed in figures 11–12. The positive conclusion we can make is that the Wigner distribution is compatible with the histogram for the largest p (figure 12(h)), where the classical dynamics is highly chaotic, (most probably) mixing, with large Kolmogorov entropy (I).

It appears that Berry's assumptions are justified for ergodic systems, but not necessarily for systems in the transition region. His derivation certainly does not apply to integrable systems, and by the continuity argument also not to their neighbourhoods. In fact, near an integrable system one expects a clustering of diabolical points (=degeneracy points in the energy × 2-dimensional parameter space, at which level sheets have a conical intersection), increased number of cones with large opening angle, and therefore non-negligible contributions to $P(S)$ from level sheets with distant conical intersections. The latter fact would imply a failure of the applicability of a local ensemble in parameter space, which would change the result $P(S) \propto S$ for small S, because the distribution of diabolical points cannot be considered as uniform anymore.

We feel that the situation here is similar to the question of the ensembles in the foundations of statistical mechanics, where, after all, the ensembles and their properties are derived from the dynamics. The ergodic theory gives a dynamical explanation for the statistical properties of (few-body) systems, and tells us thereby which ensembles are appropriate. Similarly, we believe that level spacing distribution $P(S)$ is determined by the dynamical properties of the system, and if ensembles of neighbouring systems (in the space of Hamilton systems) are used to derive $P(S)$, then a dynamical justification of these ensembles is required.

† More precisely, Berry predicts $P(S) \propto S$ as $S \to 0$ for all nonintegrable cases, with the possibility that the domain of validity shrinks to zero as the system approaches the integrable case. In this case his prediction would refer to the fine structure near $S=0$ which is almost hopeless to verify numerically. Of course, the implication that the linear level repulsion law implies Wigner's distribution is not a part of Berry's prediction, but follows from our derivation. However, we have reasons to expect that Berry's prediction holds for very chaotic systems, e.g. ergodic, but not necessarily for nearly integrable KAM systems, and other systems in the intermediate region (see below). For more details see Berry (1983b).

We expect that the exponent ν changes continuously with a generic perturbation of an integrable system. If so, is there any (local) universality concerning the dependence of the critical exponent ν on the perturbation parameter ε, for sufficiently small ε? A hint is provided by our billiard as a generic perturbation of the circular disc. In figure 13 we plot ν against parameter p_0 (see table 2). Within the numerical accuracy the data are compatible with a linear dependence $\nu = \text{constant} \times p$. Now, notice that the proper perturbation parameter in our case is $\varepsilon = p^2$, because all perturbation expansions have the leading term of order p^2. (This is so because changing the sign of λ, or of p, does not change the physics of our billiard.) Therefore, we may conjecture that for sufficiently small generic perturbations of an integrable system the critical exponent ν is proportional to the square root of the perturbation parameter ε,

$$\nu = \text{constant} \times \sqrt{\varepsilon}. \tag{57}$$

This is not ill defined, because there is no freedom of reparametrisation, since we

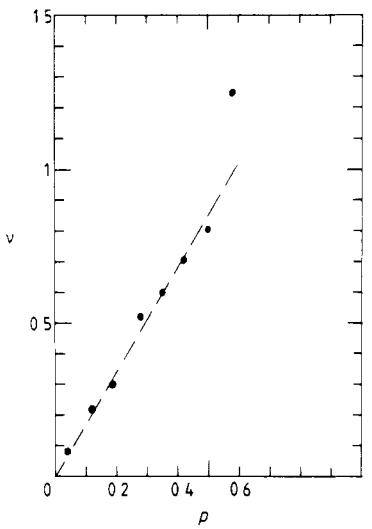

Figure 13. The critical exponent against the parameter p, according to the data of the histograms (table 2).

Table 2. Data for figures 11, 12: p_0 is the centre of the p interval from which the levels were taken to obtain a histogram, $\lambda_0 = (1/\sqrt{2}) \tan p_0$, σ is the calculated dispersion of the histogram, ν the inferred critical exponent (see figure 11) and h the value of the classical K entropy, $h = h(p_0)$, according to Robnik (1983).

Histogram	p_0	λ_0	σ	ν	h
a	0.04	0.03	0.91	0.08	0.000
b	0.12	0.08	0.80	0.22	0.002
c	0.19	0.14	0.76	0.30	0.04
d	0.27	0.20	0.65	0.52	0.18
e	0.35	0.26	0.63	0.60	0.27
f	0.42	0.32	0.60	0.70	0.35
g	0.50	0.39	0.57	0.80	0.40
h	0.58	0.46	0.47	1.25	0.42

require the leading terms of the perturbation expansions to be linear in ε. More numerical examples are needed to test this conjecture, and we need a theoretical explanation.

7. Concluding remarks

Let us summarise our major message. Delocalisation of wavefunctions as a consequence of strong mixing of states occurs near avoided crossings. Since they appear also in nearly integrable systems with regular classical motion, they cannot be regarded as consequences of the classical chaos, individually. They are, however, increasingly more probable as a system goes through a stochastic transition and becomes a highly chaotic classical system. The avoided crossings are thus a consequence of the classical chaos only in a statistical sense, i.e. as an overall property of the spectrum. (This has been exemplified in § 6.) Even in a classical chaotic system with no tori there may exist localised wavefunctions, although they are less probable with increasing Kolmogorov entropy (cf Noid *et al* 1980).

We thereby conclude that increasingly more states become chaotic when the corresponding classical system becomes nonintegrable and chaotic. By a chaotic state we mean one with a nonlocalised wavefunction, having a random appearance and approximately microcanonical probability density. We have not calculated the transition probabilities for the transitions between chaotic states, but it is qualitatively clear that the matrix elements between states with random wavefunctions are much lower than those between ordered, localised states.

We make the following prediction (cf Marcus 1980a): for systems which have predominantly chaotic states (in a certain energy region) the oscillator strengths for the transitions to such states will be drastically diminished and randomly distributed, in contrast to the transitions between ordered, localised states. In the latter case the oscillator strengths follow some systematic rule (determined by the approximate symmetries of the states).

In the statistical sense the classical chaos *is* a criterion to predict existence of chaotic states. The generic situation for Hamilton systems with a smooth potential is then characterised by a critical energy E_{crit}: below E_{crit} the classical motion is (almost) integrable and the spectral lines obey some deterministic rule, while above E_{crit} the classical motion is chaotic and the oscillator strengths are randomly distributed. The quadratic Zeeman effect in the hydrogen atom (Robnik 1981, 1982, Harada and Hasegawa 1983) seems to be an example for this phenomenon.

We stress the fact that the above criterion may not be applied to individual states. In § 5 we have shown examples of localised wavefunctions for a chaotic classical system. In fact, such exceptions of individual ordered states are expected, in particular for the low states (depending on $\hbar$), even in classical chaotic systems. This leads to 'surprising' localisations (Hose and Taylor 1983) for the general reasons described in § 5, and has important implications for the stability of molecules, since the chemical bond requires a localised wavefunction.

Finally, our numerical results suggest that the level repulsion law (50) and the level spacing distribution (51) change continuously with a generic perturbation of an integrable Hamilton system. They are characterised by a single parameter, namely the critical exponent ν, which vanishes for integrable cases (Poisson distribution). We conjecture a local universality: for a sufficiently small perturbation parameter ε we

expect $\nu = \text{constant} \times \sqrt{\varepsilon}$. Our results are compatible with the prediction $\nu = 1$ (Wigner distribution) for ergodic systems.

Acknowledgments

This work was supported by the Deutsche Forschungsgemeinschaft.

Appendix

We consider the Schrödinger eigenvalue problem,

$$\Delta\psi_E + (E - U)\psi_E = 0, \tag{A1}$$

where $U = U(q)$ is the potential in the d-dimensional configuration space, assumed bounded from below, i.e. $U(q) \geq U_{\min}$, and $\psi_E = \psi_E(q)$ is the eigenfunction. By a nodal cell we mean a finite, simply connected region bounded by the $(d-1)$-dimensional nodal surfaces (i.e. bounded by the zero set of $\psi_E(q)$). We show that there exists a lower bound $V_{\min}(E)$ (depending on the energy E) to the volume of a nodal cell of $\psi_E(q)$.

The estimate of $V_{\min}$ follows by the comparison of the eigenvalue problem (A1) with the Laplace eigenvalue problem with Dirichlet's boundary conditions on the nodal cell $D \subseteq \mathbb{R}^d$. The point is that $\psi_E(q)$ is a solution of (A1) on D with different boundary condition, namely $\psi_E/\partial D = 0$, but with same energy E. The Laplace problem subject to these conditions follows by replacing the potential $U(q)$ by its lower limit $U_{\min}$, i.e.

$$\Delta\varphi_{E'} + (E' - U_{\min})\varphi_{E'} = 0, \tag{A2}$$

where $\varphi_{E'}(q)$ with the eigenvalue $E' - U_{\min}$ is now the ground state of the Laplace operator on D. But among all domains D of constant volume the ground eigenvalue is the smallest for the d-dimensional sphere (Robnik 1980b). Therefore,

$$E' - U_{\min} \geq \pi\gamma_{0,1}^2[\Gamma(d/2+1)]^{-2/d}V^{-2/d}, \tag{A3}$$

where V is the volume of the nodal cell D, Γ the gamma function, and $\gamma_{0,1}$ the first zero of the Bessel function of order zero, i.e. $J_0(\gamma_{0,1}) = 0$.

Notice that $E \geq E'$, because $U(q) \geq U_{\min}$ and $\langle\psi|U(q) - U_{\min}|\psi\rangle \geq 0$. From this and (A3) we obtain the final result

$$V(D) \geq V_{\min}(E) = [(E - U_{\min})/\pi\gamma_{0,1}^2]^{-d/2}/\Gamma(d/2+1), \tag{A4}$$

where the equality is satisfied only if $U(q) = U_{\min}$ on D and D is a d-dimensional sphere.

In the special case of a plane box ($d = 2$, $U(q) = 0$), we have $U_{\min} = 0$ and the area $\mathcal{A}$ of a nodal cell obeys the inequality

$$\mathcal{A} \geq \mathcal{A}_{\min} = \pi\gamma_{0,1}^2/E, \tag{A5}$$

where the equality holds only for a circular nodal cell.

References

Arnold V I 1980 *Mathematical Methods of Classical Mechanics* (New York: Springer)
Arnold V I and Avez A 1968 *Ergodic Problems of Classical Mechanics* (New York: Benjamin)
Baltes H P and Hilf E R 1978 *Spectra of Finite Systems* (Mannheim: BI Wissenschaftsverlag)

Berry M V 1977a *Phil. Trans. R. Soc.* A **287** 237
—— 1977b *J. Phys. A: Math Gen.* **10** 2083
—— 1981 *Ann. Phys.* **131** 163–216
—— 1983a in *Proc. July 1981 'Les Houches' Summer School on Chaotic Behaviour of Deterministic Systems* (Amsterdam: North-Holland)
—— 1983b in *The Wave-Particle Dualism* ed S Diner *et al* (Amsterdam: Reidel)
Berry M V and Tabor M 1977 *Proc. R. Soc.* A **356** 375–94
Berry M V and Wilkinson M 1983 *Proc. Phys. Soc.* to appear
Brody T A, Flores J, French J B, Mello P A, Pandey A and Wong S S M 1981 *Rev. Mod. Phys.* **53** 385–479
Clark C W and Taylor K T 1980 *J. Phys. B: At. Mol. Phys.* **13** L737
Courant R and Hilbert D 1968 *Methoden der Mathematischen Physik* (Berlin: Springer)
Harada A and Hasegawa H 1983 *J. Phys. A: Math. Gen.* **16** L259
Helleman R H G 1980 in *Fundamental Problems in Statistical Mechanics* vol 5, ed E G D Cohen (Amsterdam: North-Holland) pp 165–233
Hogg T and Huberman B A 1982 *Phys. Rev. Lett.* **48** 711
Hose G and Taylor H S 1983 *Phys. Rev. Lett.* **51** 947
Jaffé C and Reinhardt W P 1982 *J. Chem. Phys.* **77** 5191
Korsch H-J 1983 *Phys. Lett.* **97A** 77
Krahn E 1925 *Math. Ann.* **94** 97
Landau L D and Lifshitz E M 1975 *Quantum Mechanics* (London: Pergamon)
Lazutkin V F 1973 *Math. Izv. USSR* **37** 186–216
Lewis Z W, Bosanac S and Korsch H-J 1984 *J. Phys. A: Math Gen.* **17** 523
McDonald S W and Kaufman A N 1979 *Phys. Rev. Lett.* **42** 1189
Marcus R A 1980a *Horizons in Quantum Chemistry* ed K Fukui and B Pullman (Dordrecht: Reidel) p 107
—— 1980b *Ann. NY Acad. Sci.* **357** 159
Mather J N 1982 *Ergodic Theory and Dynamical Systems* **2** 3–4
Noid D W, Koszykowsky M L and Marcus R A 1979 *J. Chem. Phys.* **71** 2864
—— 1981a *Classical, Semiclassical and Quantum Mechanical Problems in Mathematics, Chemistry and Physics* ed K Gustavson and W P Reinhardt (New York: Plenum) p 133
—— 1981b *Ann. Rev. Phys. Chem.* **32** 267–309
Noid D W, Koszykowski M L, Tabor M and Marcus R A 1980 *J. Chem. Phys.* **72** 6169
Ramaswamy R and Marcus R A 1981 *J. Chem. Phys.* **74** 1379
Robnik M 1980a *Phys. Lett.* **80A** 117
—— 1980b *J. Phys. A: Math. Gen.* **13** L349
—— 1981 *J. Phys. A: Math Gen.* **14** 3195
—— 1982 *J. Physique Colloque C2* **43** C2–45
—— 1983 *J. Phys. A: Math. Gen.* **16** 3971
—— 1984 *J. Phys. A: Math. Gen.* **17** 109
Robnik M and Zaslavsky G M 1983 *Phys. Rev. Lett.* to be submitted
Shirts R B and Reinhardt W P 1982 *J. Chem. Phys.* **77** 5204
Sinai Ya 1976 *Introduction to Ergodic Theory* (Princeton: University Press)
Strelcyn J-M 1982 *These de Doctorat d'Etat, Universitè Pierre et Marie Curie*
—— 1983 *Private communication*
von Neumann J and Wigner E 1929 *Phys. Z.* **30** 467
Whiteman K J 1977 *Rep. Prog. Phys.* **40** 1033
Wigner E 1967 *SIAM Rev.* **9** 1
Zaslavsky G M 1977 *Zh. Eksp. Teor. Fiz.* **73** 2089
—— 1979 *Sov. Phys.-Usp.* **22** 788
—— 1981 *Phys. Rep.* **80** 157–250